Neutron capture on ^{179}Ta

M. Schumann and F. Käppeler
Forschungszentrum Karlsruhe, Institut für Kernphysik, Postfach 3640, D-76021 Karlsruhe, Germany
(Received 16 March 1999; published 6 July 1999)

The (n,γ) cross section of the unstable isotope ^{179}Ta ($t_{1/2}=1.82\pm0.03$ yr) has been measured at thermal energies by means of the activation method. The ^{180}Hf$(p,2n)$ reaction was used for the production of ^{179}Ta, and thin samples of 4 and 20 ng were obtained by the electrospraying technique. From irradiations with and without Cd absorbers the thermal cross section $\sigma_{th}=932\pm62$ b and the corresponding resonance integral $I_{res}=1216\pm69$ b could be determined. [S0556-2813(99)02308-0]

PACS number(s): 25.40.Lw, 27.70.+q, 82.80.Bg, 97.10.Cv

I. ^{180}Ta PUZZLE

The origin of ^{180}Ta, nature's rarest isotope, represents a persisting astrophysical puzzle [1]. One of the most promising scenarios for the production of ^{180}Ta is the slow neutron capture process (*s* process), which takes place during stellar He burning at temperatures of 150 to 300 MK. With a typical neutron capture time scale of a few months, the resulting reaction path follows the valley of β stability. Whenever an unstable isotope with a half-life of about 1 yr is encountered this reaction path exhibits a characteristic branching due to the competition between neutron captures and β decays. In the mass region between Hf and W two branchings at $A=179$ and 180 lead to the production of ^{180}Ta as sketched in Fig. 1. Though both branches towards ^{180}Ta are comparably weak, they may well suffice to produce most or even all of its very small natural abundance [1].

While the second branch at $A=180$ has been shown to contribute about 20% [2,3], the alternative branching at ^{179}Hf was found to be more prolific. As pointed out by Takahashi and Yokoi [4] the terrestrially stable ^{179}Hf becomes unstable against β^- decay under *s*-process conditions. In spite of the faster back decay, a small equilibrium abundance of ^{179}Ta is established in this way. Even though neutron capture on this small ^{179}Ta abundance leads predominantly to the short-lived ground state ($t_{1/2}=8.15$ h), the quasistable isomer ($t_{1/2}>10^{15}$ yr) is still sufficiently produced to account for the observed ^{180}Ta. Since most neutron captures feed the short-lived ground state of ^{180}Ta, the *s* process provides the rare ^{180}W as well, thus adding another constraint for the *s*-process contributions to the $A=180$ nuclei.

Among other parameters, such as neutron flux and temperature at the stellar site, the actual contribution from the above production mechanism depends on the neutron capture cross section of the unstable branch point nucleus ^{179}Ta. This work represents the first step towards an experimental determination of the stellar neutron capture rate of ^{179}Ta. It describes the successful production and preparation of appropriate samples which could be used for measuring the yet unknown thermal (n,γ) cross section via activation.

II. EXPERIMENTAL METHOD

A. Principle

In view of the high specific ^{179}Ta activity of 4×10^{13} Bq/g, traditional techniques for (n,γ) cross section measurements at keV neutron energies are practically excluded since these require sample masses of about 1 g. Presently, the activation method remains the only possible way for determining this cross section. Because of its unsurpassed sensitivity, this technique allows us to use samples in the sub-μg region with a correspondingly reduced γ-ray background. However, an activation measurement provides only the partial cross section to the short-lived ground state (see Fig. 1). To obtain the full cross section information this result can be complemented by a statistical model calculation of the relative cross sections leading to the isomer and ground state of ^{180}Ta, respectively.

The definition of the ^{179}Ta sample as well as the determination of the activity produced in the thermal irradiation can be conveniently performed via γ spectroscopy with a HPGe detector. At keV energies, however, the induced activity is too weak for being detected in the γ-ray background from the sample, thus requiring the more sensitive detection of the decay electrons with a suited β spectrometer. With respect to this condition, a sufficiently thin ^{179}Ta sample had to be prepared. The relevant decay properties of ^{179}Ta and ^{180}Ta are summarized in Table I.

B. Sample preparation

The required ^{179}Ta was efficiently produced via the ^{180}Hf$(p,2n)$ reaction using a 27 MeV proton beam from the Karlsruhe compact cyclotron. A water-cooled Hf foil of 1 mm thickness and 1 cm diameter was irradiated for 12 h at a

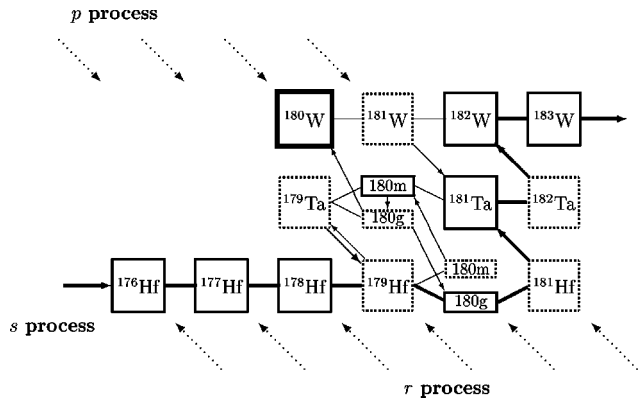

FIG. 1. The possible *s*-process production of ^{180}Ta and ^{180}W via the branching of the reaction path at $A=179$.

TABLE I. Adopted decay properties of ^{179}Ta and ^{180}Ta from Refs. [16,17].

Decay mode	Photons		Electrons	
	E_γ (keV)	I_γ (%)	$E_{\rm bin}$ (keV)	I_e (%)
^{179}Ta (1.82±0.03 yr); EC[a]				
Hf L	7.0–10.7	18.8±1.0	10–11	43.5
Hf $K\alpha_2$	54.611	13.5±0.4	43–46	1.4
Hf $K\alpha_1$	55.790	23.6±0.7	51–56	0.73
Hf $K\beta_2$	63.166	7.70±0.22	60–63	0.075
Hf $K\beta_1$	65.211	2.00±0.06		
^{180}Ta (8.152±0.006 h); EC/β^-				
Hf L	7.0–10.7	23.0±3.0	6.18	63±4
W L	7.4–11.4	0.65±0.17	6.53	1.5±0.4
Hf $K\alpha_2$	54.611	20.4±0.8	28.05	5.0±0.3
Hf $K\alpha_1$	55.790	35.7±1.3	34.07	0.68±0.2
W $K\alpha_2$	57.981	0.17±0.03	44.8	3.42±0.14
W $K\alpha_1$	59.318	0.29±0.05	45.7	0.029±0.009
Hf $K\beta$	63.2	15.0±0.6	82.13	12.3±0.6
W $K\beta_1$	67.155	0.097±0.016	90.8	3.05±0.15
W $K\beta_2$	69.342	0.025±0.004	91.5	1.6±0.5
$\gamma_{\rm EC}$	93.331	0.0451±0.0016	92.86	0.87±0.05
γ_{β^-}	103.6	0.0081±0.0024	100.8	0.40±0.12
			103.0	0.12±0.04

[a]EC=electron capture.

beam current of 30 μA. The proton energy was adjusted at the maximum of the ^{180}Hf(p,2n) cross section (900 mb at $E_{\rm proj}-E_{\rm thres}=10$ MeV), taking advantage of the fact that ^{180}Hf is the most abundant hafnium isotope. More importantly, this reaction avoids the coproduction of a long-lived ^{182}Ta impurity which would have been impossible to separate chemically. Any further enhancement of the ^{179}Ta yield required an enriched ^{180}Hf target. However, this material was only available as hafnium oxide which does not tolerate high beam currents. After irradiation, a number of short-lived by-products were allowed to decay during a storage time of 6 months until manageable levels between 10^4 and 10^8 Bq were reached. Approximately 1.4 μg of ^{179}Ta were produced in this way.

The chemical separation of the ^{179}Ta fraction from the inert hafnium matrix and from the remaining radioactive impurities (mostly long-lived Hf and Lu isotopes as well as a number of lighter reaction products including Zr, Y, Nb, Co, Zn, and Mn nuclei) was performed by liquid-liquid column chromatography. The best separation factors for this procedure were obtained by combining methylisobutylketone (MIBK) for the organic stationary phase and an acidic mixture of 1 mol H_2SO_4 and 0.06 mol HF for the polar eluant [5]. Figure 2 shows the setup for the separation. Presaturated MIBK was dispensed in the column together with inert Teflon powder of mesh 40/60 serving as the carrier of the stationary phase. Excessive MIBK was washed out with the H_2SO_4/HF mixture. The column was sealed by two frits to protect the load.

The irradiated Hf foil was dissolved in hot concentrated sulfuric acid and diluted with hydrofluoric acid and water to obtain the required concentration of 1 mol H_2SO_4 and 0.06 mol HF. This radioactive hydrous phase was then passed through the column at a flow rate of 0.2 ml/min by controlling the valve at the outlet, and collected in polypropylene bottles in 1–3 ml steps. Tantalum and possibly small amounts of other elements are accumulated in the MIBK covering the Teflon powder, while hafnium and the majority of the detectable impurities leave the column with the hy-

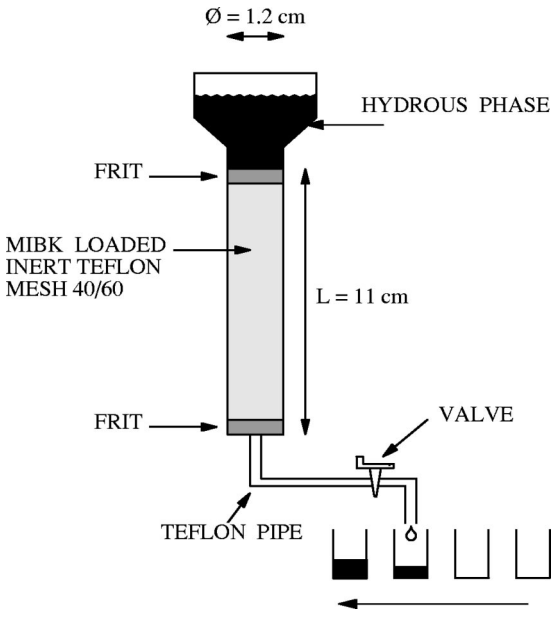

FIG. 2. Scheme of the chromatographic separation using a column with inert Teflon of mesh 40/60 as the MIBK carrier. The radioactive hydrous phase passes gravitationally through the column at a flow rate of 0.2 ml/min adjusted by the valve at the outlet.

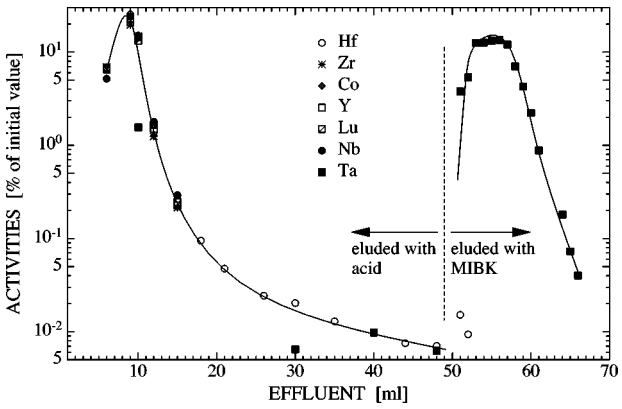

FIG. 3. Efficiency obtained in separating the tantalum fraction from coproduced radioactive impurities. The uncertainties of the plotted values range between 1% and 20% according to the respective activities.

drous phase. The separation factor was further improved by rinsing the column with excessive hydrous eluant. Finally, the tantalum fraction was extracted with MIBK.

The separation is illustrated in Fig. 3, where the measured γ activities are plotted versus the outflow from the column. Error bars have been omitted in this plot but are typically between 1% and 20%. Obviously, all impurities behave chemically similar and are hardly kept by the column, whereas tantalum is quantitatively accumulated. After optimization of this procedure, 80%–90% of the produced ^{179}Ta could be collected in the tantalum fraction. The achieved separation factors are summarized in Table II.

From this tantalum fraction a sufficiently thin homogeneous sample was prepared by electrospraying [6] onto an aluminum foil of 0.125 mm thickness and 99.999% chemical purity. As shown in Fig. 4 the solution was sprayed from the tip of a small syringe mounted at 5–10 mm distance above the sample. In this way, the extracted jet of fine droplets produced an image of about 2 mm diameter on the sample. By heating the carrier foil to 200 °C the droplets react chemically to form a solid layer. Since a sample diameter of 8–10 mm was best suited for the subsequent measurement, a larger surface was covered by means of a movable table.

After the electrosprayed layer was completely dry, the actual sample was punched out of the aluminum backing. Finally, it was covered with a 20 μg thick carbon foil in order to avoid any further losses. In total, two samples containing about 4 and 20 ng ^{179}Ta could be prepared (Table III).

The number of ^{179}Ta atoms in the samples was obtained from the respective x-ray yields measured with a calibrated 40 ccm HPGe detector. From these spectra one obtains

TABLE II. Separation factors in the column chromatography of tantalum (in units of 10^4).

Element	Hf	Zr	Co	Y	Lu	Nb	Re
Separation factor	62	>0.78	>0.34	>2.5	>2.5	>3.3	>1.4

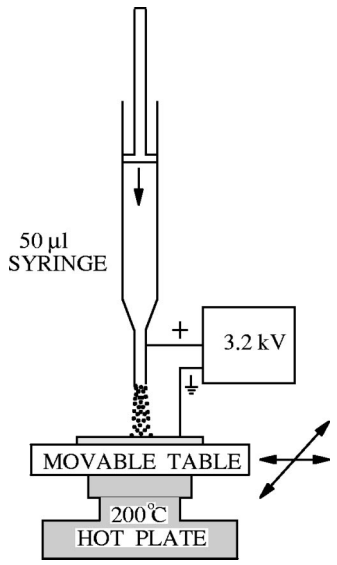

FIG. 4. Setup for the sample production via electrospraying. The ^{179}Ta solution is ejected as a jet of fine droplets, which mostly evaporate before deposition on the aluminum backing. Homogeneous samples of 8 and 10 mm diameter were produced by moving the sample backing.

$$N^{179}=\frac{c_{K\alpha,K\beta}}{\lambda^{179}t_m I_{K\alpha,K\beta}\epsilon_{K\alpha,K\beta}}, \tag{1}$$

where c denotes the number of events in the K x-ray lines, I the intensities per decay, ϵ the detection efficiency, λ^{179} the decay constant of ^{179}Ta, and t_m the dead-time-corrected duration of the activity measurement. The sample masses were inferred from the mean of the measured intensities of the $K\alpha$ and $K\beta$ x-ray lines (Table I).

III. MEASUREMENTS

A. Cadmium-difference method

The neutron spectrum of a thermal reactor consists essentially of the true thermal flux with energies below 0.2 eV and the epithermal component covering the range from 0.2 eV to 0.5 MeV. The fast flux with $E_n>0.5$ MeV can be neglected in the present study since the capture cross sections are comparably small in this energy range. Accordingly, the reactor spectrum can be written as

$$\Phi(E)dE=\Phi_{th}\frac{E\exp(-E/kT_0)}{(kT_0)^2}dE+\Phi_{\rm epi}\frac{\Delta(E)}{E}dE, \tag{2}$$

where $\Phi_{\rm th}=\int\Phi_{\rm th}(E)dE$ denotes the integrated thermal flux, $\Phi_{\rm epi}$ the epithermal flux per logarithmic energy interval, $\Delta(E)$ the joining function defining the epithermal cutoff at the transition to the thermal part [7], and $T_0=20.44$ °C the standard neutron temperature corresponding to a thermal energy $E_0=0.0253$ eV.

In such a spectrum, the activation C, which corresponds to the ratio of activated and target nuclei,

TABLE III. Characterization of the ^{179}Ta samples.

Sample	Diameter (mm)	Activity (Bq)	Number of ^{179}Ta atoms	^{179}Ta mass (ng)
TA1	8	$(1.5\pm0.02)\times10^{5}$	$(1.25\pm0.08)\times10^{13}$	3.71
TA2	10	$(9.07\pm0.15)\times10^{5}$	$(7.52\pm0.20)\times10^{13}$	22.4

$$C=\frac{N_{\rm act}}{N_{\rm target}}=\Phi_{\rm th}\sigma_{\rm th}+\Phi_{\rm epi}\sigma_{\rm epi}, \tag{3}$$

can be expressed in terms of the Maxwellian-averaged thermal and epithermal cross sections

$$\sigma_{\rm th}=\int_0^\infty \sigma(E)E\ \exp(-E/kT_0)/(kT_0)^2\,dE$$

and $\sigma_{\rm epi}=\int_0^\infty \sigma(E)\Delta(E)/E\,dE$, respectively. From Eq. (3) it follows that the thermal cross section can only be determined if the epithermal contribution to the induced activity is determined as well.

The cadmium-difference method [8] has been used to measure the epithermal contribution, by repeating the activation with the sample canned in a Cd absorber. Below 0.5 eV, the large absorption cross section of Cd ensures that the sample is shielded from thermal neutrons. Accordingly, the measured activity is only due to the epithermal part. By combining the result of both activations, the thermal cross section can be expressed as

$$C_{\rm th}=C-F_{\rm Cd}C_{\rm Cd}, \tag{4}$$

with $C_{\rm Cd}=\Phi_{\rm epi}I_{\rm res}$, where $I_{\rm res}=\int_{E_{\rm Cd}}^\infty \sigma(E)\Delta(E)/E\,dE$ is the resonance integral [8]. The correction factor $F_{\rm Cd}$ considers deviations from an ideal cutoff behavior and depends on the Cd thickness, the geometry, cross section shape, and sample thickness (see below).

From Eq. (3) one obtains

$$\frac{C_{\rm th}}{C_{\rm Cd}}=\frac{C}{C_{\rm Cd}}-F_{\rm Cd}, \tag{5}$$

$$\frac{\sigma_{\rm th}}{I_{\rm res}}\frac{\Phi_{th}}{\Phi_{\rm epi}}=R_{\rm Cd}-F_{\rm Cd}, \tag{6}$$

$$\sigma_{\rm th}=\frac{\Phi_{\rm epi}}{\Phi_{\rm th}}I_{\rm res}(R_{\rm Cd}-F_{\rm Cd}). \tag{7}$$

While the cadmium ratio $R_{\rm Cd}=C/C_{\rm Cd}$ is directly measured via the activations with and without Cd absorber, the flux ratio can be determined by the simultaneous activation of suited monitor foils with well-known cross sections. One obtains

$$\sigma_{\rm th}^{^{179}{\rm Ta}}=\frac{(R_{\rm Cd}-F_{\rm Cd})^{^{179}{\rm Ta}}}{(R_{\rm Cd}-F_{\rm Cd})^{\rm mon}}\left(\frac{\sigma_{\rm th}}{I_{\rm res}}\right)^{\rm mon} I_{\rm res}^{^{179}{\rm Ta}}, \tag{8}$$

$$I_{\rm res}^{^{179}{\rm Ta}}=\frac{C_{\rm Cd}^{^{179}{\rm Ta}}}{C_{\rm Cd}^{\rm mon}}I_{\rm res}^{\rm mon}. \tag{9}$$

The Co and Au monitors used in the present experiment exhibit significantly different $\sigma_{\rm th}/I_{\rm res}$ ratios. This allows to reduce the uncertainties in the flux ratio and to check for possible differences in the neutron spectrum between the thermal and epithermal activation.

Finally, the above equations have to be modified to account for the sample thickness, which may affect the measured activities:

$$C_{\rm Cd}=G_{\rm epi}\Phi_{\rm epi}I_{\rm res}, \tag{10}$$

$$C_{\rm th}=G_{\rm th}F_{\rm th}\Phi_{\rm th}\sigma_{\rm th}, \tag{11}$$

where G is the self-absorption correction and F the correction for flux depression due to neutron absorption in the Al backing and in the monitor foils. With these corrections one finally has

$$I_{\rm res}^{^{179}{\rm Ta}}=\frac{C_{\rm Cd}^{^{179}{\rm Ta}}}{C_{\rm Cd}^{\rm mon}}\frac{G_{\rm epi}^{\rm mon}}{G_{\rm epi}^{^{179}{\rm Ta}}}I_{\rm res}^{\rm mon}, \tag{12}$$

$$\sigma_{\rm th}^{^{179}{\rm Ta}}=\frac{(G_{\rm th}F_{\rm th})^{\rm mon}}{(G_{\rm th}F_{\rm th})^{^{179}{\rm Ta}}}\frac{(R_{\rm Cd}-F_{\rm Cd})^{^{179}{\rm Ta}}}{(R_{\rm Cd}-F_{\rm Cd})^{\rm mon}}\frac{C_{\rm Cd}^{^{179}{\rm Ta}}}{C_{\rm Cd}^{\rm mon}}\sigma_{\rm th}^{\rm mon}. \tag{13}$$

B. Reactor activations and induced activities

Both samples, TA1 and TA2, were irradiated three times in the Triga Mark I reactor in Heidelberg at a thermal flux of $\Phi_{\rm th}\approx10^{13}$ s^{-1} cm^{-2}. One of these activations was performed without Cd absorber with the sample canned in a flat Al cylinder with a total height of 2 mm, 11.5 mm outer diameter, and 0.5 mm thick walls. The 0.01 mm thick monitor foils, a gold disk of 6 mm diameter and a cobalt disk of 10 mm diameter, were attached to the outside of the 0.2 mm thick top and bottom parts of the Al can. For the activations with Cd absorber, this entire sandwich was put inside cylindrical Cd absorbers with 0.5 and 1 mm thick walls, respectively. Each of these activations lasted for about 14 h.

The induced activation can be determined via

$$C^i=\frac{N_{\rm act}^i}{N_{\rm target}^i t_{\rm irr} f_b}, \tag{14}$$

where i denotes the ^{179}Ta, Au, and Co samples. The number of target nuclei was determined from the weights of the

TABLE IV. Compilation of uncertainties.

Source of uncertainty	Uncertainty (%)		
	Ta	Au	Co
Activity measurement			
Statistics c_γ	1.0–1.9	0.2	0.2–0.5
Waiting time f_w	0.1	$\leqslant$0.1	$\leqslant$0.1
Counting time f_m	$\leqslant$0.1	$\leqslant$0.1	$\leqslant$0.1
Pileup K_p	0.7–1.0	0.2–0.3	0.1–0.2
Summation $K_{\rm sum}$	$\leqslant$0.1	$\leqslant$0.1	$\leqslant$0.1
Absorption K_γ	$\leqslant$0.1	$\leqslant$0.1	$\leqslant$0.1
Line intensity I_γ	3.5	0.1	$\leqslant$0.1
Detector efficiency ϵ_γ	2.0	1.0	1.0
Reactor irradiation and related quantities			
Sample definition $N_{\rm target}$	2.6	0.7	0.3
Decay during activation f_b	$\leqslant$0.5	$\leqslant$0.1	$\leqslant$0.1
Neutron self-shielding $G_{\rm epi}$	$\leqslant$0.5	2.0	3.5
$G_{\rm th}$	$\leqslant$0.1	0.5	$\leqslant$0.5
Flux depression $F_{\rm Cd}$	$\leqslant$10	$\leqslant$1.5	$\leqslant$3.0
Resonance integral $I_{\rm res}$		1.8	2.0
Thermal cross section $\sigma_{\rm th}$		0.1	0.16
Total uncertainties			
Activations C	5.0–5.2	1.3	1.2
Cadmium ratios $R_{\rm Cd}$	3.2–3.6	1.0	0.6
Resonance integral $I_{\rm res}$	5.8		
Thermal cross section $\sigma_{\rm th}$	6.7		

monitor foils and from the ^{179}Ta activities, respectively (Table III). The decay during the irradiation in the constant reactor flux is considered by the factor $f_b^i = [1-\exp(-\lambda_i t_{\rm irr})]/(-\lambda_i t_{\rm irr})$. The number of activated nuclei is evaluated from the intensities of the corresponding lines in the γ-ray spectra of the activated samples, which were taken with the same HPGe detector used for characterizing the ^{179}Ta samples,

$$N_{\rm act}^i = \frac{c_\gamma}{I_\gamma \epsilon_\gamma f_w f_m} K_\gamma K_p K_{\rm sum}. \tag{15}$$

In analogy to Eq. (1), c_γ, I_γ, and ϵ_γ are the number of events in the investigated line, the absolute intensity per decay of this line, and the corresponding detector efficiency. The factor $f_w = \exp(-\lambda_i t_w)$ corrects for the decay between irradiation and activity counting, and $f_m = 1-\exp(-\lambda_i t_m)$ accounts for the decay during the activity measurement, t_m being the dead-time-corrected duration of this measurement. The correction for γ self-absorption, $K_\gamma = 1 - \exp(-\mu d)/\mu d$, considers the sample thickness d and the respective absorption coefficient μ. Minor corrections concerning pileup effects (K_p) and the problem of cascade summing ($K_{\rm sum}$) contribute very little to the overall uncertainty (Table IV).

C. Data analysis

The required input data for these final equations are discussed in the following.

(i) *Correction factors.* For the extremely thin tantalum sample, the thermal and epithermal correction factors for self-absorption are negligible. Since gold is often used as a standard, theoretical as well as experimental data are available for this monitor [8–10]. For the present setup, these are $G_{\rm epi}({\rm Au}) = 0.51$ and $G_{\rm th}({\rm Au}) = 0.98$. For cobalt, theoretical data have to be used which yield a negligible correction for the thermal value and an epithermal correction $G_{\rm epi}({\rm Co}) = 0.83$ [11]. This is in good agreement with the measured value of 0.86, which is obtained by comparing the activities of the two monitor foils.

The thermal flux depression due to neutron absorbers in the vicinity of the sample (Al, Au, and Co) was estimated according to Ref. [12], and can be neglected for the current geometry.

The corrections $F_{\rm Cd}({\rm Au})$ and $F_{\rm Cd}({\rm Co})$ were adopted from the literature [8,13]. Since the cross section of ^{179}Ta is unknown around the 0.5 eV cutoff energy, $F_{\rm Cd}({\rm Ta})$ is difficult to determine. However, assuming that the major part of the epithermal activation is due to resonances with energies far above the cadmium cutoff energy, the correction factor $F_{\rm Cd}({\rm Ta})$ can be neglected. The uncertainty due to this assumption is discussed below (see Table IV).

(ii) *Cross sections.* The thermal neutron capture cross sections and the respective resonance integrals were adopted from Refs. [7,13]: $\sigma_{\rm th}({\rm Co}) = 37.18 \pm 0.06$ b, $\sigma_{\rm th}({\rm Au}) = 98.65 \pm 0.10$ b, $I_{\rm res}({\rm Co}) = 74.00 \pm 0.13$ b, and $I_{\rm res}({\rm Au}) = 1550 \pm 25$ b. All these data contribute very little to the uncertainty of the present measurement.

(iii) *Activities.* The induced ^{198}Au and ^{60}Co activities of the monitor foils could be determined from the γ-ray spectra by means of the respective lines at 412 and 1171 keV. Because of the relatively high intensities, these measurements were performed at a sample-detector distance of 93 cm. In this way, the count rates were sufficient to achieve good statistics, but low enough to yield negligible pileup and summation corrections ($C_p = C_{\rm sum} = 1$). The detector efficiency was measured between 20 and 1200 keV by a set of calibrated γ sources. In the usual log-log plot, the efficiency could well be fitted by a straight line above 150 keV.

The weaker ^{180}Ta activity was measured by placing the sample at a distance of 13.6 cm from the HPGe detector. In this geometry, the efficiency was determined at γ energies of 59.6 and 88.0 keV by means of calibrated ^{241}Am and ^{109}Cd sources. The extrapolation to the 93.3 keV γ transition in the ^{180}Ta decay required a somewhat larger uncertainty than in the well-defined region above 150 keV.

The experimental spectrum of the activated sample TA1 is shown in Fig. 5. In spite of the very small sample mass, the signatures from the ^{179}Ta decay in the sample as well as from the activated ^{180}Ta are quite clear. For the cross section analysis, only the 93.3 keV line was used because of the poor statistics in the second ^{180}Ta line at 103.6 keV. The significant background underneath both lines is due to Compton scattering of a ^{24}Na activity produced by (n,α) reactions in the Al backing.

D. Uncertainties

The experimental uncertainties of the thermal cross section, the resonance integral, and of the ratio $I_{\rm res}/\sigma_{\rm th}$ of ^{180}Ta

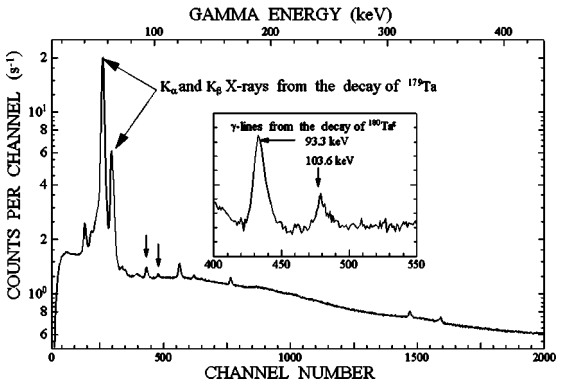

FIG. 5. The γ-ray spectrum measured between 10 and 440 keV after irradiation of the smaller sample TA1. The characteristic lines from the decay of ^{180}Ta are given in the inset.

were evaluated by quadratic summation of the contributions from the various quantities in Eqs. (12) and (13). This means that all quantities were considered independent of each other. Though this is not strictly true for the cadmium ratios and for C_{Cd}, the respective correlations are weak enough to justify this assumption.

All uncertainties are summarized in Table IV. For the part of the activity measurements, relatively large uncertainties are due to the limited counting statistics and to the decay intensity of the 93.3 keV line. The uncertainties related to the reactor irradiation are determined by the number of ^{179}Ta atoms in the sample as well as by the contributions from the monitor samples. In particular, the correction for flux depression carries sizable uncertainties. In the case of ^{60}Co it is caused by the extrapolation of the value from Ref. [13] to the finite thickness of the actual monitor foil. For ^{179}Ta, this uncertainty was difficult to estimate since the cross section shape is unknown. The assumption $F_{\mathrm{Cd}}(\mathrm{Ta})=1$ yields $I_{\mathrm{res}} > \sigma_{\mathrm{th}}$, indicating significant resonance absorption. Therefore, the $1/v$ contribution to the resonance integral should be small, and an estimated uncertainty of 10% should be sufficiently conservative. In view of the large cadmium ratio, this uncertainty has little impact on the final cross section though. Larger uncertainties due to resonances in the cutoff region between 0.1 and 0.7 eV could be excluded by the activation with the 0.5 mm thick Cd absorber.

IV. THERMAL CROSS SECTION AND RESONANCE INTEGRAL

The results obtained in the activations with and without the Cd absorbers are listed in Table V, where the first two lines represent the combined analysis of the activations without and with the 1 mm thick absorber. The good agreement of the resonance integrals based on both monitors confirms that the thermal part of the spectrum was efficiently removed.

TABLE V. Experimental results of the various thermal activations of ^{179}Ta.

Cd absorber	Monitor	$I_{\mathrm{res}}(E_{\mathrm{Cd}})$ (b)	$\sigma_{\mathrm{th}}(E_0)$ (b)	$I_{\mathrm{res}}/\sigma_{\mathrm{th}}$
1 mm	^{197}Au	1205±72	979±68	1.19±0.06
	^{60}Co	1170±70	916±62	1.28±0.07
0.5 mm	^{60}Co	1737±103		

TABLE VI. Final results for the ^{179}Ta$(n_{\mathrm{th}},\gamma)^{180g}$Ta reaction.

$I_{\mathrm{res}}\vert_{0.55\ \mathrm{eV}}^{2\ \mathrm{MeV}}$ (b)	$\sigma_{\mathrm{th}}(E_0)$ (b)	$I_{\mathrm{res}}/\sigma_{\mathrm{th}}$
1216±69	932±62	1.23±0.06

The main reason for using the thinner absorber was to test the cross section shape of ^{179}Ta in the Cd cutoff region for obtaining an estimate of the uncertainty in F_{Cd}. The obvious difference indicates a remaining thermal component. The thermal cross sections could not be deduced in this case, but this activation provides an important argument. Because of the remaining thermal component, the Cd cutoff energy is shifted towards the epithermal part of the spectrum. Since the corresponding deviation in $(I_{\mathrm{res}}/\sigma_{\mathrm{th}})_{\mathrm{Ta}}$ is in agreement with the deviations of the monitor foils, possible ^{179}Ta resonances in the critical interval at the Cd cutoff energy are excluded, hence confirming the experimental $(I_{\mathrm{res}}/\sigma_{\mathrm{th}})_{\mathrm{Ta}}$ ratio.

The thermal cross section is given for $E_0=0.0253$ eV, the usual value for the peak of the thermal spectrum. The resonance integral in Table V is an experimental quantity and, therefore, depending on the Cd cutoff energy according to

$$I_{\mathrm{res}}^{\mathrm{expt}}=\int_{E_{\mathrm{Cd}}}^{\infty}\frac{\sigma(E)}{E}dE.$$

Resonance integrals are usually tabulated for integration limits of 0.55 eV and 2 MeV. For a $1/v$ absorber, experimental values can be transformed to these limits [12] via

$$I_{\mathrm{res}}\vert_{0.55\ \mathrm{eV}}^{2\ \mathrm{MeV}}=kI_{\mathrm{res}}^{\mathrm{expt}}.$$

Since tabulated resonance integrals of the monitors have been used in deriving the experimental value for ^{179}Ta, the corresponding correction yields

$$I_{\mathrm{res}}\vert_{0.55\ \mathrm{eV}}^{2\ \mathrm{MeV}}=\frac{k^{\mathrm{Ta}}}{k^{\mathrm{mon}}}I_{\mathrm{res}}^{\mathrm{expt}}.$$

For a 1 mm thick Cd absorber, $E_{\mathrm{Cd}}=0.68$ eV [12] leads to rather small corrections of $k^{\mathrm{Ta}}/k^{\mathrm{Au}}=1.035$ and $k^{\mathrm{Ta}}/k^{\mathrm{Co}}=1.013$ with uncertainties below 2%. With this definition the final results in Table VI were determined as the weighted mean of the values obtained with the Au and Co monitors.

V. OUTLOOK

The present investigation has demonstrated that ^{179}Ta can be efficiently produced by proton bombardment of natural Hf at 27 MeV, chemically purified, and prepared in form of very thin samples. Activation of these samples has allowed to measure the thermal (n,γ) cross section and the resonance integral of ^{179}Ta with uncertainties of 6.6% and 5.7%, re-

spectively. In a second step, these techniques will be used to study the stellar (n,γ) rate as well. As a result of the weaker neutron fluxes and smaller cross sections at keV energies, the sensitivity of the experiment has to be improved correspondingly. Test activations of the existing samples in the quasi-stellar neutron spectrum obtained via the ^{7}Li$(p,n)^{7}$Be reaction [14,15] have already shown that successful measurements will be possible with about 10 times higher sample masses. Such samples can be produced with the described techniques.

[1] Z. Németh, F. Käppeler, and G. Reffo, Astrophys. J. **392**, 277 (1992).
[2] H. Beer and R. Macklin, Phys. Rev. C **26**, 1404 (1982).
[3] S. Kellogg and E. Norman, Phys. Rev. C **31**, 1505 (1985).
[4] K. Takahashi and K. Yokoi, At. Data Nucl. Data Tables **36**, 375 (1987).
[5] M. Schumann, Report No. FZKA-5985, Forschungszentrum Karlsruhe, 1997.
[6] A. Lally and K. Glover, Nucl. Instrum. Methods Phys. Res. A **223**, 259 (1984).
[7] J. Mughabghab, in *Neutron Cross Sections* (Academic Press, New York, 1984), Vol. 1, Pt. B.
[8] K. Beckurts and K. Wirtz, *Neutron Physics* (Springer, Berlin, 1964).
[9] D. Albert, Kernenergie **5**, 154 (1962).
[10] M. Brose, Nukleonik **6**, 134 (1963).
[11] H. Yamamoto and K. Yamamoto, J. Nucl. Sci. Technol. **2**, 421 (1965).
[12] F. Bensch and C. Fleck, *Neutronenphysikalisches Praktikum* (Bibliographisches Institut, Mannheim, 1968).
[13] A. Simonits *et al.*, J. Radioanal. Nucl. Chem. **81**, 397 (1984).
[14] H. Beer and F. Käppeler, Phys. Rev. C **21**, 534 (1980).
[15] W. Ratynski and F. Käppeler, Phys. Rev. C **37**, 595 (1988).
[16] ENDF Evaluation, National Nuclear Data Center, Brookhaven National Laboratory, on-line access: bnlnd2.dne.bnl.gov.
[17] E. Browne and R. Firestone, *Table of Radioactive Isotopes* (Wiley, New York, 1986).